Fault Detection and Severity Assessment in PMSMs Using Search Coils Exploiting Machine's Symmetry

Marcos Orviz
Dept of Elect. Computer & System Engineering
University of Oviedo
Gijón, 33204, Spain
orvizmarcos@uniovi.es

David Reigosa
Dept of Elect. Computer & System Engineering
University of Oviedo
Gijón, 33204, Spain
diazdavid@uniovi.es

Hyeon-Jun Lee
Department of Electrical Engineering
Korea University
Seoul, Korea
lhjoon14@gmail.com

Jigyun Jeong
Department of Electrical Engineering
Korea University
Seoul, Korea
jjg0402@korea.ac.kr

Sang Bin Lee
Department of Electrical Engineering
Korea University
Seoul, Korea
sangbinlee@korea.ac.kr

Fernando Briz
Dept of Elect. Computer & System Engineering
University of Oviedo
Gijón, 33204, Spain
fernando@isa.uniovi.es

***Abstract*—Online fault detection is a highly appealing feature for electric drives. Search coils (SCs) have been shown to be a viable option for demagnetization detection for PMSMs. This paper analyses the use of SCs for the detection, classification, and severity assessment of other type of faults, including static, dynamic, and mixed eccentricity, and bearings misalignment. While these faults can be present for practically all electric machine types, the proposed method is specific for PMSMs as it relies on the measurement of magnet field using SCs.[1]**

Keywords—eccentricity, misalignment, search coil, zero-sequence voltage, differential voltage

I. Introduction

Permanent magnet synchronous machines (PMSMs) are often the preferred option in applications like hybrid and electric vehicles (HEVs, EVs), wind generation, servodrives, etc. as they outperform other type of electric machines in terms of torque and power densities, efficiency, and controllability, with cost and reliability being their main disadvantages. PMSMs can suffer from several types of faults, demagnetization of permanent magnets (PMs) being perhaps the main concern, being specific of this machine design. Other types of faults as dynamic, static, or mixed eccentricities, interturn short-circuit faults, bearings misalignment, and load unbalance (i.e., torque/speed pulsations produced by the load); can also occur, but they are common to most machine types.

Table I summarizes the most relevant fault detection techniques reported in the literature for the specific case of PMSMs.

Motor current signature analysis (MCSA) is one of the most extended methods for online fault detection as it does not require extra sensors or signals. It can be used for detection of both rotor and stator faults [1]-[5] but has not been reported its use for load fault detection. MCSA is based on the variation of the machine current harmonic content when a fault occurs. Unfortunately, different faults often produce similar harmonic content which makes difficult fault classification and severity assessment [1]. Also the current signature can be affected by the current regulators for the case of current regulated drives. Therefore, MCSA is typically combined with other techniques, e.g., motor voltage signature analysis (MVSA) [1],[2] or linear discriminant analysis (LDA) [1], for reliable fault classification and severity estimation.

Use of Hall-effect sensors has been proven to be a feasible option for online detection and classification of rotor (except static eccentricity and misalignment) and load defects [6]-[8]; their use for stator fault detection has not been reported in the literature. These techniques require the use of analog Hall-effect sensors. Even if such sensors can be already present for control purposes, their characteristics and spatial location might not match with the requirements for detection of rotor, stator and load defects.

High frequency signal injection (HFI) methods have been shown to be effective for online detection and classification of both rotor (except misalignment) and stator faults [9]-[12], their use for load fault detection has not been reported. Main limitations are the additional induced losses, noise, and vibration due to the HF signal injection.

Search coils (SCs) can be used for online detection and classification of rotor (except misalignment), stator and load faults [13]-[15]. The main advantages of SCs based methods is that they are insensitive to machine parameters. However, SCs based methods cannot work at zero or low speeds, and they are invasive (require SC installation).

In [13], detection and classification of partial demagnetization, dynamic eccentricity and load unbalance faults is carried out using a single SC, severity assessment of the detected faults not being possible. In [14], the use of one

[1]This work was supported in part by the Research, Technological, Development and Innovation Programs of the Spanish Ministry of Science and Innovation under grant PID2019-106057RB-I00.

Table I: Classification of PMSMs' Faults and Literature on Fault Detection Techniques

	Rotor faults					Stator faults	Load faults
	Demagnetization	Eccentricity			Misalignment	Inter-turn Short-circuit	Load Unbalance
		Dynamic	Static	Mixed			
MCSA	✓[1],[2]	✓[3]	✓[1],[3]	✓[1],[3]	✓[5]	✓[1],[4]	×
Hall-Effect	✓[6]-[8]	✓[8]	×	✓[7],[8]	×	×	✓[7]
HFI	✓[9]	✓[10]	✓[10]	✓[10]	×	✓[11],[12]	×
SCs	✓[13]-[15]	✓[13],[14]	✓[14]	✓[14]	×	✓[14]	✓[13]

Table II: Test Machine Parameters	
Machine type	IPMSM
Number of slots, n_s	36
Number of pole pairs, P	3
Rated Speed	1500 rpm
Rated Power	2.2 kW
Rated Current	11.6 A
Number of turns per SC	5

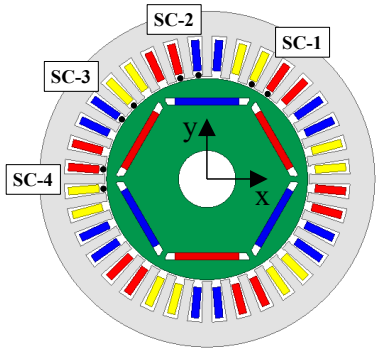

Fig. 1: Test machine model.

SC per stator slot was proposed for detection, classification, and quantification of partial demagnetization, dynamic, static and mixed eccentricity, and inter-turn short-circuit faults. Detection and severity assessment of a partial demagnetization fault (only for the case of one PM) of a PMSM using SCs has been reported in [15]; two or three SCs (depending on the number of stator slots and rotor poles of the machine) were required in this case.

This paper focuses on PMSMs fault detection, classification and severity assessment using SCs. The method presented in [15] will be extended for the detection, classification and quantification of static/dynamic/mixed eccentricity, and bearings misalignment faults. Fault detection will be based on the harmonic content variation of the zero-sequence (three SCs being required) or differential voltage (two SCs being required) provided by the SCs, while fault quantification will rely on the magnitude variation of these signals. Main advantage of this method compared to [13] and [14] is the use of a null fault detection signal during healthy operation which increases as the fault level does, thus allowing fault severity assessment (which is not feasible in [13]) with a lower number of SCs than the method proposed in [14].

The paper is organized as follows: Section II describes two potential implementations of fault detection using SCs. Section III develops the procedure for fault identification through harmonic content prediction. Section IV focuses on the implementation of the methods. Sections V presents finite element (FE) simulation results. Conclusions are finally given in Section VI.

II. Fault Detection Methods

Table II shows the main characteristics of the IPMSM test machine, its FEM model being shown in Fig. 1. The machine is equipped with 4 SCs that will allow the implementation of the zero-sequence and the differential voltage approaches, both are briefly described following [15].

1) Zero-sequence voltage based implementation

This implementation uses three SC voltages shifted 120 electrical degrees (see SC-1, SC-2 and SC-3 in Fig. 1). In a perfectly balanced machine, the zero-sequence voltage component (1) will be zero [15]. Faults will often result in an asymmetric behavior of the machine, the zero-sequence voltage not being null anymore. It will be shown that the harmonic content of V_0 provides information about the type of fault. The method requires three sensors and is limited to machines having stator slots shifted 120 electrical degrees.

$$V_0=1/3\cdot(V_{SC1}+V_{SC2}+V_{SC3}) \quad (1)$$

$$V_{diff}=V_{SC1}-V_{SC4} \quad (2)$$

2) Differential voltage based implementation

The induced voltage in two SCs shifted 360 electrical degrees (see SC-1 and SC-4 in Fig. 1) will be identical if the machine is perfectly balanced. The differential voltage between both SCs, see (2), will consequently reveal asymmetries in the machine. Similar to the V_0 approach, the harmonic content of V_{diff} will be shown to provide information of the type of fault. The method requires only two sensors, but it is limited to machines having slots shifted 360 electrical degrees.

In [15], a viability analysis of both methods for demagnetization detection showed that for slots-poles configurations not producing V_0, V_{diff} will exist, and the other way around. Therefore, at least one of the two methods can always be used, independently of the configuration of the machine. It will be shown in this paper that the same conclusion applies for other fault types.

III. Harmonic Content Prediction for Fault Identification

As discussed in the previous section, the harmonic content of V_0 and V_{diff} provides information about the fault type. This section presents a mathematical model to predict the harmonic content of both V_0 and V_{diff} for the different type of faults. The voltage induced in a SC consist of two components, which are induced by the PM flux and the armature current respectively [14]. Under healthy operation, both components will induce a sinusoidal voltage in a SC, the resulting SC voltage being also sinusoidal. As shown in [15], the effect of a fault (partial demagnetization) can be modelled by the product of the ideal induced voltages in the SC by a window signal that emulates the effect of the fault on the SCs' voltages. Fig. 3a shows the

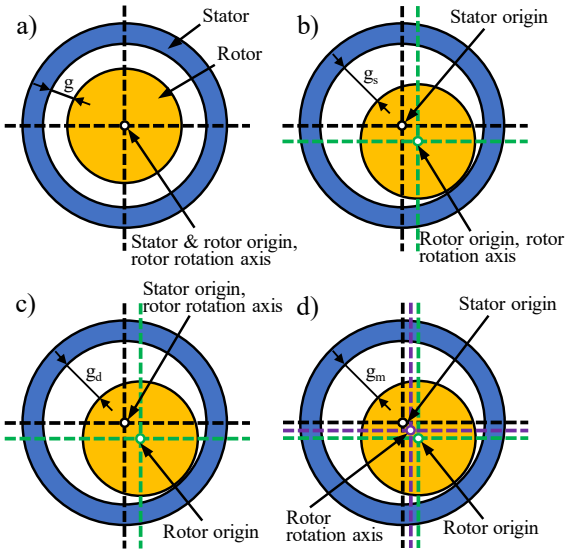

Fig. 2: Schematic representation of different types of eccentricities. (a) Healthy machine. (b) Static eccentricity. (c) Dynamic eccentricity. (d) Mixed eccentricity.

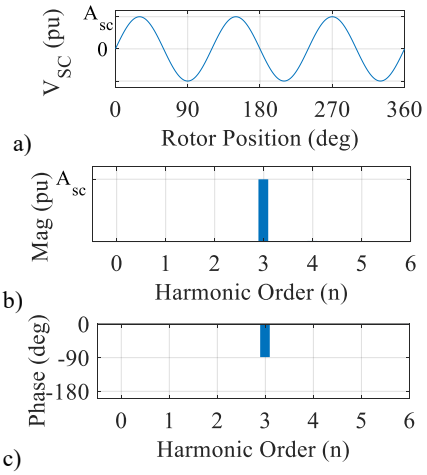

Fig. 3: a) Individual SC voltage, b) magnitude and c) phase of the FFT of V_{SC} for a 3 pole pair PMSM (see Fig. 1).

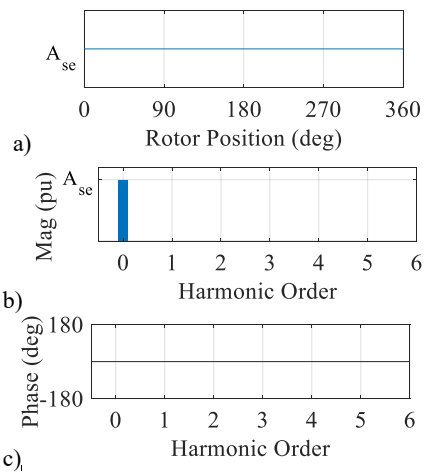

Fig. 4: a) Window signal for static eccentricity, b) magnitude and c) phase of the FFT of the window signal.

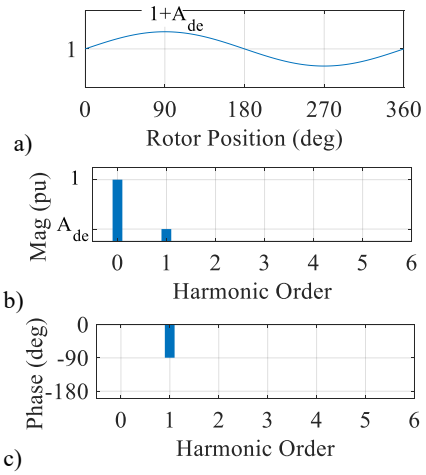

Fig. 5: a) Window signal for dynamic eccentricity, b) magnitude and c) phase of the FFT of the window signal.

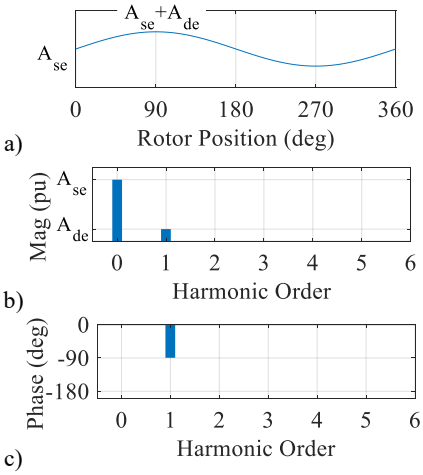

Fig. 6: a) Window signal for mixed eccentricity, b) magnitude and c) phase of the FFT of the window signal.

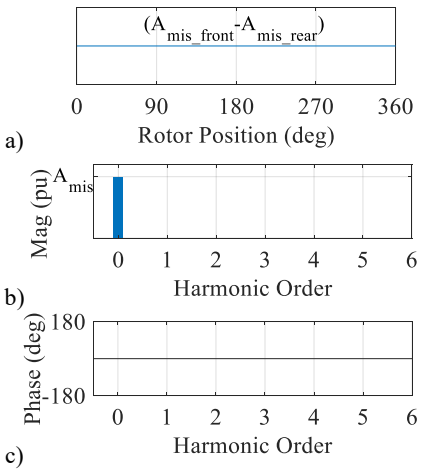

Fig. 7: a) Window signal for bearings misalignment, b) magnitude and c) phase of the FFT of the window signal.

ideal induced voltage in a single SC, the amplitude and phase of its harmonic content being shown in Fig. 3b and c, respectively, where n is the harmonic order normalized to the machine mechanical frequency and A_{sc} is the SC voltage amplitude. The window signals, and their respective harmonic content, that allow to model the effect of dynamic/static/mixed eccentricity, bearings misalignment and load unbalance faults will be analysed in this section.

1) *Window functions*

a. *Static Eccentricity*

Fig. 2a shows a schematic representation of a healthy machine with constant airgap, g. Static eccentricity consists of the displacement of both the geometrical and the rotation center of the rotor respect to the stator (see Fig. 2b); the air-gap in front of each SC, g_s, will be constant during time, but different for each SC. For static eccentricity, a constant window signal, with a magnitude of A_{se} can be used to model this effect on each SC (see Fig. 4a), where A_{se} represents the ratio between the airgap in healthy conditions, g, and the airgap under a static eccentricity fault, g_s, (see (3)), i.e., $A_{se}<1$ if $g<g_s$ (the magnitude of the SC voltage will be lower than in healthy operation), and $A_{se}>1$ if $g>g_s$ (the magnitude of the SC voltage will be higher than in healthy operation). Fig. 4b and c show the magnitude and phase of the FFT of the window signal.

$$A_{se}=g_s/g \tag{3}$$

b. *Dynamic Eccentricity*

Dynamic eccentricity faults appear when the geometrical center of the rotor is displaced respect to the geometrical center of the stator and the rotational center (see Fig. 2c), the air-gap in front of each SC, g_d, will change as the machine rotates; a sine wave window function with a unity offset, amplitude A_{de} (which represents the fault severity, g/g_d, see (4)), and rotating at the machine mechanical frequency can be used to model the dynamic eccentricity effect on each SC (see Fig. 5a). Fig. 5b and c show the magnitude and phase of the FFT of the window signal.

$$A_{de}=g_d/g \tag{4}$$

c. *Mixed Eccentricity*

Mixed eccentricity consists of a combination of static and dynamic eccentricity, meaning that the geometrical center of the rotor is not coincident with either the stator geometrical center or the rotor rotational center (see Fig. 2d). In this case, the window signal that models the mixed eccentricity fault will consist of a combination of that ones used to model the

static and dynamic eccentricity faults, i.e., a sine wave with amplitude A_{de} at the mechanical frequency with an offset, A_{se}, that depends on the location of each SC (see Fig. 6a). Therefore, the harmonic content of the window signal that models the effect of a mixed eccentricity fault will consist of the combination of that of a dynamic and a static eccentricity fault (see Fig. 6b-c).

d. Bearings Misalignment

Rotor misalignment respect to stator (see Fig. 8) in a machine is typically produced by a fault in the bearings. Fig. 8a and c show the front and rear view of the rotor and the stator during a misalignment fault, respectively. It can be observed that the position of the rotor with respect to the stator on both the front and rear sides is equivalent to that of a static eccentricity fault. If the wear of the front and rear bearings is identic, the static eccentricity in the front side of the machine would be compensated by that one in the rear side, the SC voltage not being affected by the fault. On the contrary, if the wear of the front and rear bearings are not identic, the effect of the misalignment fault on the SC voltage will be the same than that of a static eccentricity. Similarly, to the static eccentricity case, the window signal for modelling the misalignment fault will consist of the mean value of the sum of a constant waveform with amplitude A_{mis_front} (static eccentricity in the front side of the machine) and a constant value with amplitude A_{mis_rear} (static eccentricity in the rear side of the machine), see Fig. 7a. The amplitude and phase of the FFT of the window signal that emulates the effect of a bearing's misalignment fault on the SC voltage are shown in Figs. 7b and c, respectively.

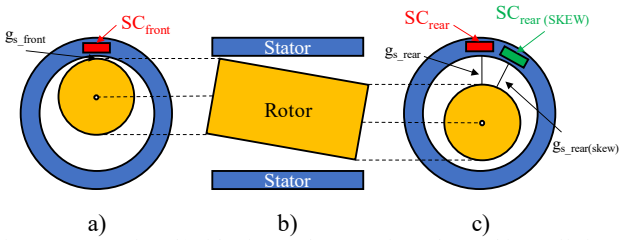

Fig. 8: a) Front view, b) side view and c) rear view of a machine suffering a misalignment fault.

e. Load Unbalance

Load unbalances are common in certain applications, e.g., washing machines [16]. In this case, stator currents, induced stator fluxes and resulting induced voltages in the SCs will not be sinusoidal anymore; components at $\omega_{re}\pm\omega_{rm}$, where ω_{re} is the machine electrical frequency and ω_{rm} is the machine mechanical frequency, will appear in the stator currents, induced stator fluxes and resulting induced voltages in the SCs. However, the same additional components will be induced in all the SCs with 120 (SC1-SC2 and SC3) or 360 (SC1 and SC4) electrical degrees phase shift between them. Therefore, the effect of the load unbalance fault will not be reflected in either V_0 or V_{diff}.

2) Harmonic Prediction through Fourier Series Analysis (FSA) and Convolution Theorem

The convolution theorem states that the Fourier transform of the product of two time-domain signals is equivalent to the convolution of the Fourier transform of each time domain signal (see equation (5)). The following procedure has been followed therefore to determine the harmonic content of both V_0 and V_{diff}: (i) obtain the harmonic content of the ideal SC voltages through FSA (see Fig. 3); (ii) obtain the harmonic content of the corresponding window signals through FSA (see Figs. 4-7); (iii) compute the harmonic content of the SC voltages under the corresponding fault (which is obtained through the product of the ideal SC voltage and the corresponding window signal) by applying the convolution theorem; (iv) obtain the harmonic content of V_0 (from the harmonic content of V_{SC1}, V_{SC2} and V_{SC3}) and V_{diff} (from the harmonic content of V_{SC1} and V_{SC4}).

$$\mathcal{F}(x(t)\cdot y(t)) = \mathcal{F}(x(t)) * \mathcal{F}(y(t)) \qquad (5)$$

Harmonic prediction of both V_0 and V_{diff} has been carried out for the different types of faults, including: dynamic, static and mixed eccentricity, and bearing misalignment. Fig. 9 shows the predicted harmonic components of both V_0 and V_{diff} for each type of fault and for the test machine that will be used in this paper, see Fig. 1 and Table II.

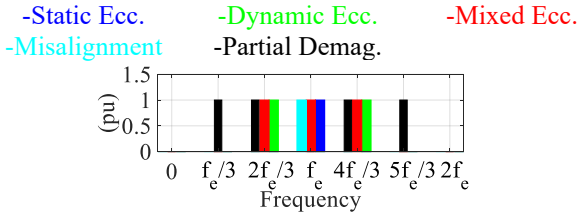

Fig. 9: Predicted harmonic components for static, dynamic and mixed eccentricity, bearings misalignment and partial demagnetization of both V_0 and V_{diff}.

Signal processing for fault identification and quantification

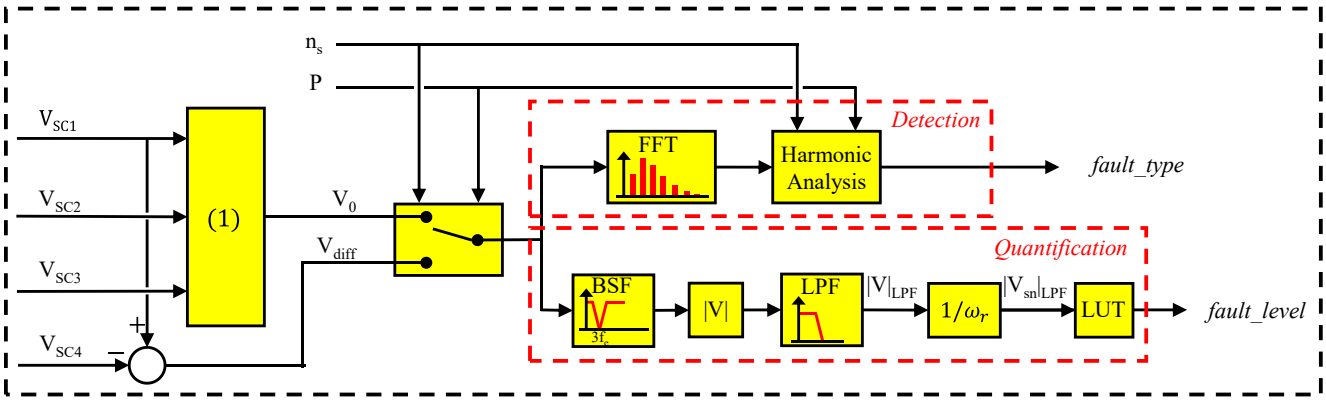

Fig. 10: Signal processing for fault detection and quantification using both $\mathbf{V_0}$ and V_{diff}.

Table III: Relationship between signal fault_type and the machine operating condition			
Condition	fault_type	Condition	fault_type
Healthy	0	Mixed Ecc.	3
Dyn. Ecc	1	Partial Demag.	4
Stat. Ecc	2	Misalignment	2

IV. Signal Processing

Fig. 10 shows the signal processing block diagram for the detection, classification and severity assessment of all fault types described in previous section using both V_0 and V_{diff}. Fault detection, classification and quantification is carried out in two steps:

Fault detection and classification: it is done by monitoring the harmonic components of V_0 and V_{diff} at $f_e/3$, $2f_e/3$, f_e, $4f_e/3$ and $5f_e/3$ (see Fig. 10); note that if the machine is healthy, the amplitude of these harmonic components is zero. Monitoring the harmonic content of V_0 and V_{diff} will allow to identify the fault type the machine is suffering; signal fault_type being obtained. Table III shows the values of fault_type depending on the fault the machine is suffering. It can be observed that fault_type is equivalent for a static eccentricity and a bearings misalignment fault; because both faults lead to identical harmonic content in V_0 and V_{diff} (see Fig. 9). This occurs since, as stated in Section III.1.d, static eccentricity and bearing's misalignment faults (with different wear in the front and the rear bearings) are identical from the point of view of the induced SC voltage, distinction between both faults not being possible.

Severity assessment: in [15], several metrics for reliable quantification of a partial demagnetization fault through both V_0 and V_{diff} were compared: total energy, E, energy of the most dominant harmonic component, E_{max}, total harmonic distortion, THD, peak value, V_{max} and mean of the absolute value $|V|_{LPF}$, the last one being found to be the most reliable. Therefore, $|V|_{LPF}$ will be used in this paper to assess the severity of each type of fault. Use of V_0 or V_{diff} will depend on the machine configuration [15]. If V_0 is used, a band-stop filter must be implemented to remove the third harmonic that is induced due to the non-ideal sinusoidal shape of the SC voltages. Then, the mean of the absolute value of V_0 or V_{diff} is calculated, $|V|_{LPF}$ being obtained. After that, $|V|_{LPF}$ is divided over the rotating speed to get a speed-normalized metric, $|V_{sn}|_{LPF}$. Finally, a look-up table will be used to obtain the fault severity signal, fault_level.

V. Simulation Results

Finite element (FE) simulations using Ansys Maxwell 2D have been used for the verification of the proposed methods.

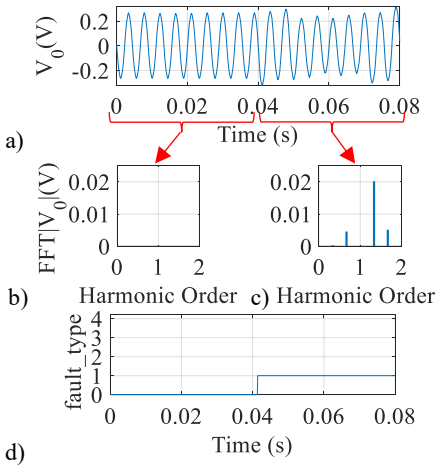

Fig. 11: a) V_0 before (t < 0.04s) and after (t > 0.04s) a dynamic eccentricity fault (50% in the positive y-axis direction), b) FFT of V_0 before and c) after the fault, d) signal fault_type. **ω_r=1500rpm, I_{dq} = 0A.**

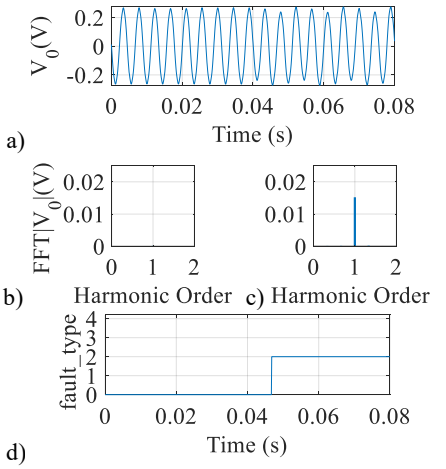

Fig. 12: Same results as in Fig. 11 for a static eccentricity fault (25% in the positive x-axis direction).

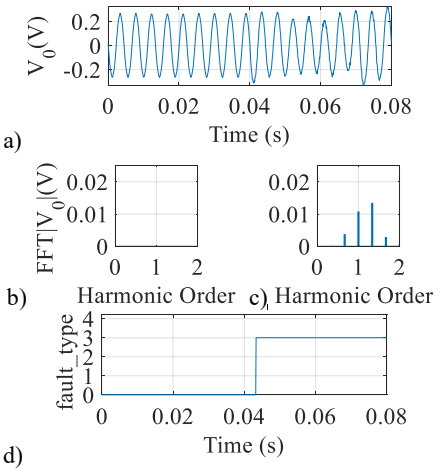

Fig. 13: Same results as in Fig. 11 for a mixed eccentricity fault (50% = 25% static eccentricity in the positive x-axis direction + 25% dynamic eccentricity in the positive y-axis direction).

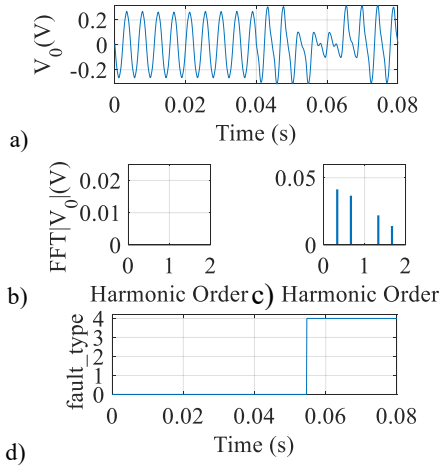

Fig. 14: Same results as in Fig. 11 for a partial demagnetization fault in one PM (100% demagnetized).

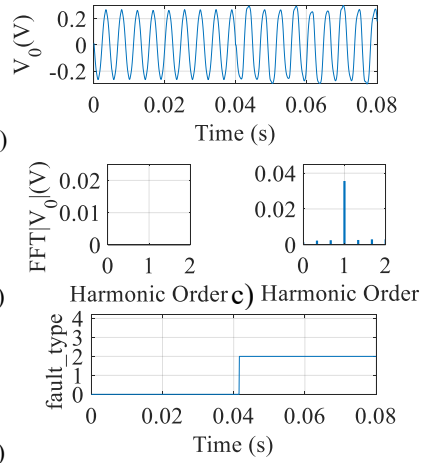

Fig. 15: Same results as in Fig. 11 for a misalignment fault (0.3º misalignment + 58% average static eccentricity in the positive y-axis direction).

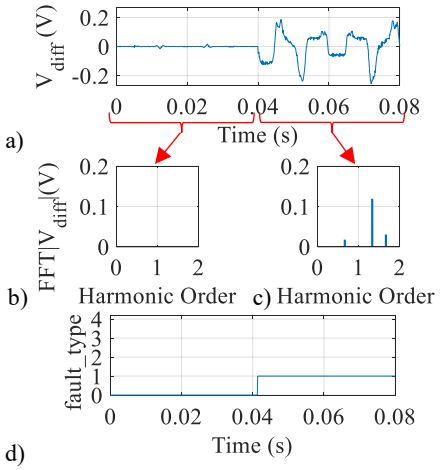

Fig. 16: Same results as in Fig. 11 for V_{diff}.

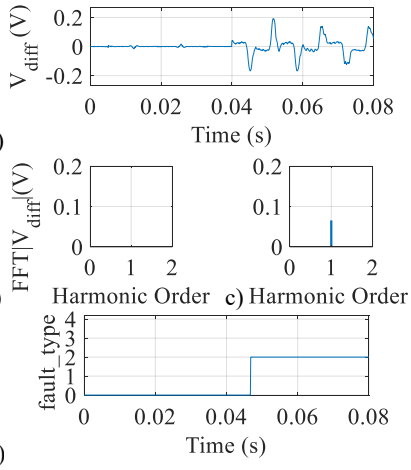

Fig. 17: Same results as in Fig. 12 for V_{diff}.

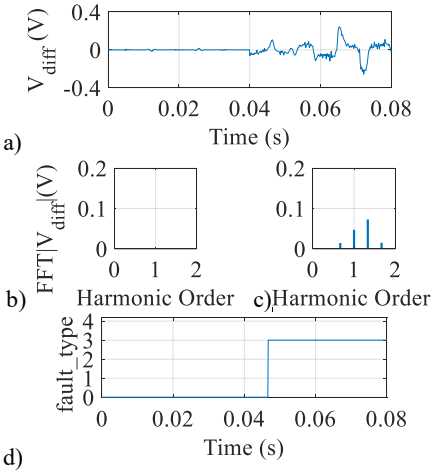

Fig. 18: Same results as in Fig. 13 for V_{diff}.

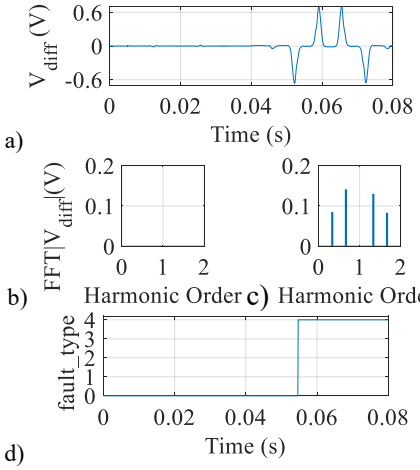

Fig. 19: Same results as in Fig. 14 for V_{diff}.

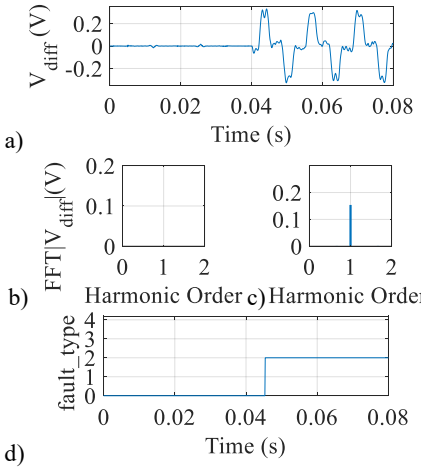

Fig.20: Same results as in Fig. 15 for V_{diff}.

The test machine shown in Fig. 1, whose main characteristics are included in Table I, will be used with this purpose. Fig. 11a shows V_0 when a dynamic eccentricity fault occurs at t = 0.04s. It can be observed that V_0 includes the third harmonic due to the non-sinusoidal waveform of the SCs. However, this additional component does not interfere with the fault detection method as components between 0 and two times the fundamental frequency will be only tracked (see Fig. 9 and 10). Fig. 11b and c show the FFT of V_0 for the case of healthy and faulty operating condition respectively. It can be observed that the harmonic content of V_0 after the dynamic eccentricity fault occurs matches with that predicted in Section III (see Fig. 9). Fig. 11d shows the fault detection signal, fault_type, which is seen to be 0 during healthy operation of the machine and turns to 1 after the dynamic eccentricity fault occurs (see Table III). Figs. 12, 13, 14, and 15 show analogous results to Fig. 11 but for static eccentricity, mixed eccentricity, partial demagnetization of one PM and bearings misalignment fault, respectively. It can be observed that the harmonic content of V_0 after each fault (see Figs. 12-15c) is in good agreement with those predictions shown in Section III (see Fig. 9). Therefore, it can be concluded that the harmonic content of V_0 allows detection of all previous described fault types. As expected, distinction between bearings misalignment and static eccentricity faults is not possible since both induce the same harmonic components in V_0 (see Figs. 17 and 20d, and Table III). Figs. 16-20 show analogous results to Figs. 12-15 but for V_{diff}. It can be observed that, similarly to V_0, the harmonic components of V_{diff} for each fault match with those predicted in Section III (see Fig. 9 and Figs. 16-20c); distinction between bearings misalignment and static eccentricity faults not being either possible in this case.

As shown in Section IV, fault severity quantification can be done by means of $|V_0|_{LPF}$ and $|V_{diff}|_{LPF}$, see Fig. 10. Fig. 21a shows $|V_0|_{LPF}$ for a dynamic eccentricity fault, while Fig. 21b shows $|V_0|_{LPF}$ vs dynamic eccentricity level; a rather linear relationship between $|V_0|_{LPF}$ and dynamic eccentricity level being readily observed. From Fig. 21b, fault severity can be online estimated, fault_level signal (see Fig. 10) being shown in Fig. 21c. It can be therefore concluded that $|V_0|_{LPF}$ allows dynamic eccentricity fault severity estimation. Fig. 22, 23 and 24 show analogous results to Fig. 21 but for static eccentricity, mixed eccentricity, and partial demagnetization of one PM, respectively, the same conclusions hold for all fault types. Fig. 25 shows analogous results to Fig. 21 but for a bearing's misalignment fault with unbalanced wear in the front and rear bearings, note that in this case the relationship between fault severity level (which is expressed as the % of static eccentricity due to the bearings' misalignment fault) and $|V_0|_{LPF}$ for a bearings misalignment fault is compared to that of a static eccentricity one, see Fig. 25b. It can be observed that the tendencies overlap for both faults, this behavior being the expected since both faults will lead to identical SC induced voltages (for the same fault severity). Therefore, the severity

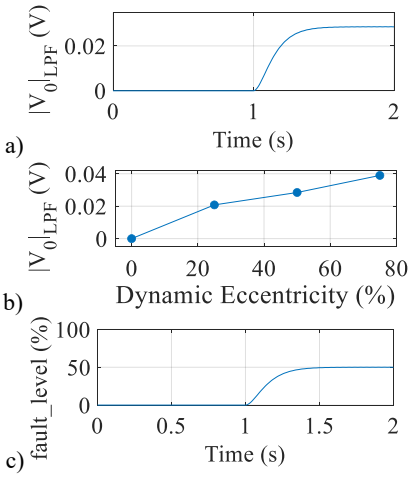

Fig. 21: a) $|V_0|_{LPF}$ before and after (t=1s) a dynamic eccentricity fault (50% in the positive y-axis direction), b) $|V_0|_{LPF}$ vs. dynamic eccentricity level and c) fault severity estimation signal, fault_level before and after (t=1s) the fault **ω_r=1500rpm, I_{dq} = 0A.**

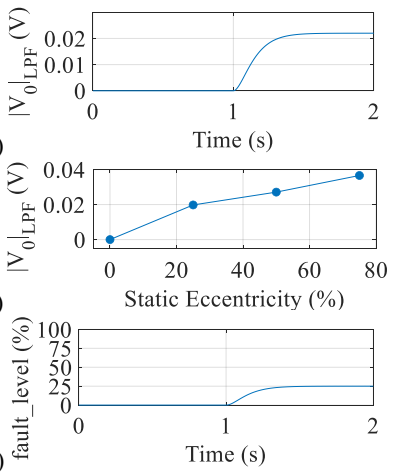

Fig. 22: Same results as in Fig. 21 for a static eccentricity fault (25% in the positive x-axis direction).

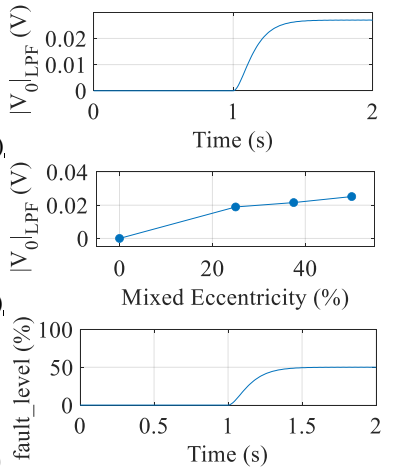

Fig. 23: Same results as in Fig. 21 for a mixed eccentricity fault (50% = 25% static eccentricity in the positive x-axis direction + 25% dynamic eccentricity in the positive y-axis direction).

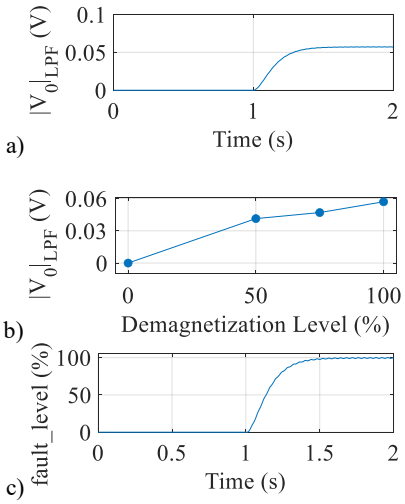

Fig. 24: Same results as in Fig. 21 for a partial demagnetization fault (100% demagnetized).

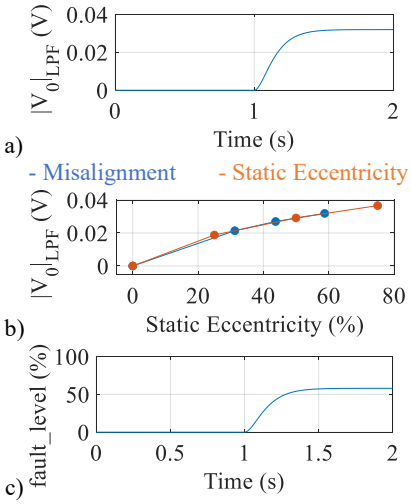

Fig. 25: Same results as in Fig. 21 for a bearings misalignment fault (0.3° misalignment + 58% average static eccentricity).

of both faults can be assessed despite distinction is not feasible.

Fig. 26-30 show analogous results to Figs. 21-25 but when using $|V_{diff}|_{LPF}$ instead of $|V_0|_{LPF}$. It can be observed that, for the different type of faults studied, $|V_{diff}|_{LPF}$ follows a linear behavior with the fault severity, quantification of the fault level being therefore possible by using this metric.

VI. Conclusions

This paper analyses SC configuration and signal processing for detection, classification, and severity assessment of different fault types, including dynamic, static, and mixed eccentricity, bearings misalignment and load unbalance. Window signals and their respective harmonic content for each of the previously mentioned faults have been defined. The use of the convolution theorem to predict the harmonic content of V_0 and V_{diff} under each type of fault from the harmonic content of the individual SC voltages and each window signal has been also presented. Techniques to first detect and later assess the severity of dynamic eccentricity, static eccentricity, mixed eccentricity, partial demagnetization of one PM and bearings misalignment faults have been presented. Fault detection is based on monitoring specific harmonic components that were previously predicted for each fault type. Severity assessment relies on the rectified and low-pass filtered value of V_0 and V_{diff}. Finite element simulation results have been provided to confirm the viability of the proposed methods for each type of fault.

References

[1] R. Z. Haddad and E. G. Strangas, "On the Accuracy of Fault Detection and Separation in Permanent Magnet Synchronous Machines Using MCSA/MVSA and LDA," in IEEE Transactions on Energy Conversion, vol. 31, no. 3, pp. 924-934, Sept. 2016, doi: 10.1109/TEC.2016.2558183.

[2] A. Usman and B. S. Rajpurohit, "Characteristic Analysis of Partial Demagnetization Faults in Surface Mounted BLDC Motors," 2020 IEEE Industry Applications Society Annual Meeting, 2020, pp. 1-8, doi: 10.1109/IAS44978.2020.9334844.

[3] B. M. Ebrahimi, J. Faiz and M. J. Roshtkhari, "Static-, Dynamic-, and Mixed-Eccentricity Fault Diagnoses in Permanent-Magnet Synchronous Motors," in IEEE Transactions on Industrial Electronics, vol. 56, no. 11, pp. 4727-4739, Nov. 2009, doi: 10.1109/TIE.2009.2029577.

[4] M. A. S. Nejad and M. Taghipour, "Inter-turn stator winding fault diagnosis and determination of fault percent in PMSM," 2011 IEEE

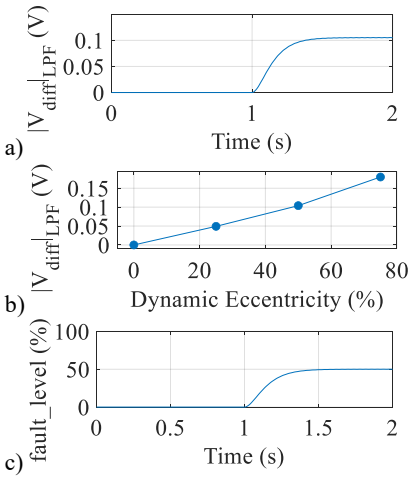

Fig. 26: Same results as in Fig. 21 for V_{diff}.

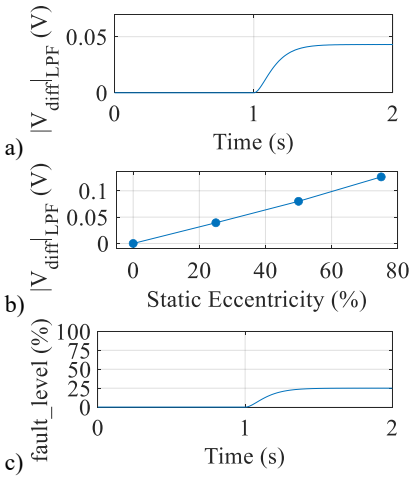

Fig. 27: Same results as in Fig. 22 for V_{diff}.

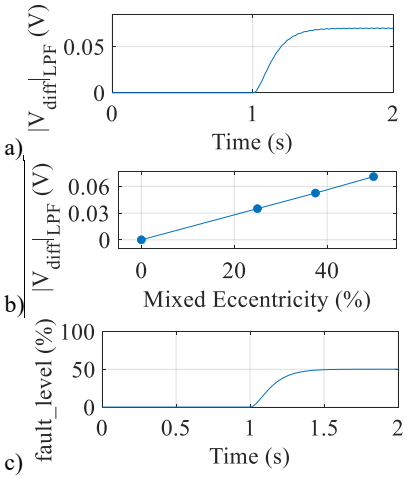

Fig. 28: Same results as in Fig. 23 for V_{diff}.

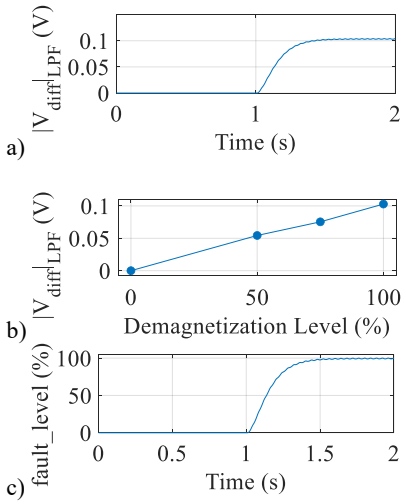

Fig. 29: Same results as in Fig. 24 for V_{diff}.

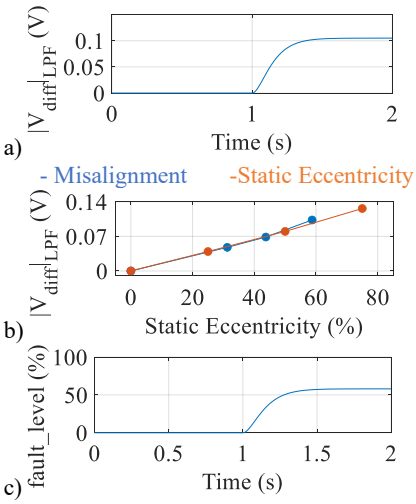

Fig. 30: Same results as in Fig. 25 for V_{diff}.

Applied Power Electronics Colloquium (IAPEC), 2011, pp. 128-131, doi: 10.1109/IAPEC.2011.5779847.

[5] B. Corne et al., "Misalignment and unbalance fault severity estimation using stator current measurements," 2017 IEEE 11th International Symposium on Diagnostics for Electrical Machines, Power Electronics and Drives (SDEMPED), 2017, pp. 247-253, doi: 10.1109/DEMPED.2017.8062363.

[6] D. Reigosa et al., "Detection of Demagnetization in Permanent Magnet Synchronous Machines Using Hall-Effect Sensors," in IEEE Transactions on Industry Applications, vol. 54, no. 4, pp. 3338-3349, July-Aug. 2018, doi: 10.1109/TIA.2018.2810123.

[7] Y. Park et al., "Online Detection and Classification of Rotor and Load Defects in PMSMs Based on Hall Sensor Measurements," in IEEE Transactions on Industry Applications, vol. 55, no. 4, pp. 3803-3812, July-Aug. 2019, doi: 10.1109/TIA.2019.2911252.

[8] Y. Park et al., "Online Detection of Rotor Eccentricity and Demagnetization Faults in PMSMs Based on Hall-Effect Field Sensor Measurements," in IEEE Transactions on Industry Applications, vol. 55, no. 3, pp. 2499-2509, May-June 2019, doi: 10.1109/TIA.2018.2886772.

[9] D. Díaz Reigosa et al., "PMSM Magnetization State Estimation Based on Stator-Reflected PM Resistance Using High-Frequency Signal Injection," in IEEE Transactions on Industry Applications, vol. 51, no. 5, pp. 3800-3810, Sept.-Oct. 2015, doi: 10.1109/TIA.2015.2437975.

[10] H. Torkaman and E. Afjei, "Comprehensive Detection of Eccentricity ault in Switched Reluctance Machines Using High-Frequency Pulse Injection," in IEEE Transactions on Power Electronics, vol. 28, no. 3, pp. 1382-1390, March 2013, doi: 10.1109/TPEL.2012.2205947.

[11] Z. Xu, J. Zhang, Y. Zhang and J. Zhao, "Winding condition monitoring for inverter-fed PMSM using high-frequency current injection," 2020 IEEE Energy Conversion Congress and Exposition (ECCE), 2020, pp. 777-782, doi: 10.1109/ECCE44975.2020.9235726.

[12] F. Briz, M. W. Degner, A. Zamarron and J. M. Guerrero, "Online stator winding fault diagnosis in inverter-fed AC machines using high-frequency signal injection," IEEE Transactions on Industry Applications, vol. 39, no. 4, pp. 1109-1117, Jul./Aug. 2003.

[13] M. S. S. Rafaq et al., "Airgap Search Coil based Identification of PM Synchronous Motor Defects," in IEEE Transactions on Industrial Electronics, doi: 10.1109/TIE.2021.3095810.

[14] Y. Da, X. Shi and M. Krishnamurthy, "A New Approach to Fault Diagnostics for Permanent Magnet Synchronous Machines Using Electromagnetic Signature Analysis," in IEEE Transactions on Power Electronics, vol. 28, no. 8, pp. 4104-4112, Aug. 2013, doi:10.1109/TPEL.2012.2227808.

[15] M. O. Zapico, D. D. Reigosa, H. J. Lee, M. S. Rafaq, S. B. Lee and F. B. del Blanco, "Demagnetization Detection in PMSMs Using Search Coils Exploiting Machine's Symmetry," 2021 IEEE Energy Conversion Congress and Exposition (ECCE), 2021, pp. 4460-4467, doi: 10.1109/ECCE47101.2021.9595756.

[16] K. Yoldaş, A. Tekin and M. Boztepe, "An Improved Speed Controller for PMSM Drive with Unbalanced Load Using Load Torque Observer," 2019 IEEE Texas Power and Energy Conference (TPEC), 2019, pp. 1-6, doi: 10.1109/TPEC.2019.8662181.